

BITCOIN VERSUS S&P500 INDEX: RETURN AND RISK ANALYSIS

A.H.NZOKEM¹

ABSTRACT. S&P 500 index is considered the most popular trading instrument in financial markets. With the rise of cryptocurrencies over the past years, Bitcoin has also grown in popularity and adoption. The paper aims to analyze the daily return distribution of the Bitcoin and S&P 500 index and assess their tail probabilities through two financial risk measures. As a methodology, We use Bitcoin and S&P 500 Index daily return data to fit The seven-parameter General Tempered Stable (GTS) distribution using the advanced Fast Fractional Fourier transform (FRFT) scheme developed by combining the Fast Fractional Fourier (FRFT) algorithm and the 12-point rule Composite Newton-Cotes Quadrature. The findings show that peakedness is the main characteristic of the S&P 500 return distribution, whereas heavy-tailedness is the main characteristic of the Bitcoin return distribution. The GTS distribution shows that 80.05% of S&P 500 returns are within -1.06% and 1.23% against only 40.32% of Bitcoin returns. At a risk level (α), the severity of the loss ($AVaR_{\alpha}(X)$) on the left side of the distribution is larger than the severity of the profit ($AVaR_{1-\alpha}(X)$) on the right side of the distribution. Compared to the S&P 500 index, Bitcoin has 39.73% more prevalence to produce high daily returns (more than 1.23% or less than -1.06%). The severity analysis shows that at a risk level (α) the average value-at-risk ($AVaR(X)$) of the bitcoin returns at one significant figure is four times larger than that of the S&P 500 index returns at the same risk.

Keywords: S&P 500 index, GST distribution, Bitcoin, value-at-risk, average value-at-risk.

1. INTRODUCTION

A cryptocurrency is a cryptographically secured digital asset, sometimes known as a cryptoasset [1]. Bitcoin was the first cryptocurrency created in 2009 by Satoshi Nakamoto. The idea behind Bitcoin was to create a peer-to-peer electronic payment system that allows online payments to be sent directly from one party to another without going through a financial institution [2]. Bitcoin was set up to replace financial institutions with a payment network based on the blockchain or distributed ledger technology. Since its inception, Bitcoin has grown in popularity and adoption and is now viewed as a viable legal tender in some countries. Its rising popularity has attracted growing interest and questions in economics and finance literature regarding the usage of Bitcoin as currency and the formation and dynamic of Bitcoin prices.

The economic appraisal of Bitcoin as currency has been done in many studies [3–7]. Like other traditional fiat currencies (Dollar, Euro, Yen, . . .), whether the bitcoin may be considered as a currency depends on its ability to fulfill the three basic functions: A medium of exchange, a store of value, and a unit of account. As a medium of exchange, Bitcoin can be used to pay someone for something or to extinguish a debt or financial obligation. However, bitcoin bears exchange rate risk (BTC/USD) [3, 4] and is not widely accepted in its current state; only five out of the top

¹ hilaire77@gmail.com.

500 online merchants accepted Bitcoin in 2016 [1]. As a store of value, Bitcoin will be worth the same as it is today. This function is also rejected in the literature [3, 4, 6, 7] as Bitcoin is unstable and has excess volatility. As a unit of count, Bitcoin can be used to compare the value of two items or to count up the total value of assets. The extreme volatility [8] of Bitcoin makes it difficult or impossible to derive the true value of a specific good in Bitcoin. Some studies [6, 8] show that the statistical properties of Bitcoin are uncorrelated with traditional asset classes such as stocks, bonds, and commodities, and the transaction analysis of Bitcoin accounts shows that Bitcoins are mainly used as an investment tool and not as a currency. A similar study [3] shows that the volatility of Bitcoin prices is extreme and almost ten times higher than the volatility of major exchange rates (US/Euro and US/Yen) and concludes that Bitcoin cannot function as a medium of exchange, but can be used as a risk-diversified tool.

The formation and dynamics of Bitcoin prices is another important aspect of the bitcoin that is studied in the literature [9–12]. Several factors affecting Bitcoin price have been identified in the literature review: market forces of Bitcoin supply and demand, Bitcoin attractiveness for investors, and global macroeconomic and financial development. The empirical results [9] show that the market forces of Bitcoin supply and demand greatly impact Bitcoin price, confirming the major role played by the standard economic model of currency in explaining Bitcoin price formation. However, the same study [9] shows that the global macro-financial development (captured by the Dow Jones Index, exchange rate, and oil price) does not significantly impact the Bitcoin price. The relationship between Bitcoin price and attractiveness has also been studied [10–12]. The attractiveness variables are the number of Google searches that used the terms bitcoin, bitcoin crash, and crisis. The findings [12] show that a Bitcoin price increase is usually preceded by an increase in the worldwide interest in Bitcoin; similarly, a fallen Bitcoin price goes along with an increase in market mistrust over a collapse of Bitcoin. In addition, another study [11] shows that the coronavirus fear sentiment, captured by hourly Google search queries on coronavirus-related words, negatively impacted the Bitcoin price (negative Bitcoin returns and high trading volume). The above discussion shows that Bitcoin is mainly used as an investment tool, not a currency. The main determinants of the Bitcoin price are market forces of Bitcoin supply and demand and Bitcoin attractiveness for investors and users. We will analyze the daily return distribution of the bitcoin and S&P 500 index and assess and compare their tail probabilities through two financial risk measures: the value-at-risk (VaR) and the average value-at-risk (AVaR). The findings will provide another perspective in understanding the distribution of the return and volatility of the bitcoin. As a methodology, We use Bitcoin and S&P 500 Index daily return data over the 2010-2023 period to fit the General Tempered Stable (GTS) distribution to the underlying data return distribution. The GTS distribution is a seven-parameter family of infinitely divisible distribution, which covers several well-known distribution subclasses like Variance Gamma distributions [13–16], bilateral Gamma distributions [17, 18] and CGMY distributions [19]. The main disadvantage of the GTS distribution is the lack of the closed form of the density, cumulative functions, and their derivatives. we use the numerical computations, which are based on the advanced Fast Fractional Fourier transform (FRFT) developed by combining the classic Fast Fractional Fourier (FRFT) algorithm and the 12-point rule Composite Newton-Cotes Quadrature. We organized the paper as follows. Section 2 provides the trend and the volatility of Bitcoin and SP 500 Index daily price data. Section 3 briefly presents the GTS distribution's theoretical framework. Section 4 develops the advanced Fast Fractional Fourier transform (FRFT) scheme.

Section 5 shows the results of the GTS Parameter Estimation from daily return data. Section 6 analyses the probability density functions and some key statistics. Section 7 develops the methodology and computes the value-at-risk and average value-at-risk.

2. BITCOIN AND S&P 500: OVERVIEW & TRENDS

The Standard & Poor's 500 Composite Stock Price Index, also known as the S&P 500, is a stock index that tracks the share prices of 500 of the largest public companies with stocks listed on the New York Stock Exchange (NYSE) and the Nasdaq in the United States. It was introduced in 1957 and often treated as a proxy for describing the overall health of the stock market or even the U.S. economy. The S&P 500 data were extracted from Yahoo Finance. The historical prices span from April 28, 2013, to June 22, 2023, and were adjusted for splits and dividends.

The Bitcoin BTC price was extracted from CoinMarketCap and spanned from January 04, 2010, to June 16, 2023. The Bitcoin and S&P 500 prices are denominated in US dollars, representing the currency in which Bitcoin and S&P 500 are the most traded.

2.1 Bitcoin's Path Compared with the S&P 500 Index's path.

Bitcoin's price fluctuations primarily stem from investors and traders. Investors use Bitcoin to store value, generate wealth, and hedge against inflation, whereas traders use it to bet against its price changes. The Bitcoin historical price used in Fig 1a starts on April 28, 2013, when Bitcoin was trading at \$134. By December 2013, the price had spiked to \$1,151 for the first and then fallen to \$698 three days later. In 2017, Bitcoin's price hovered around \$1,000 until it broke \$2,000 after mid-May and then skyrocketed to \$19,497.40 on Dec 16, 2017 (first peak in Fig 1a). The increasing demand for Bitcoin has triggered the development of cryptocurrencies to compete with Bitcoin. In 2020, the COVID-19 pandemic resulted in massive disruption in the global economy. The government policies combined with investor and trader responses accelerated the dynamic of the Bitcoin price. The bitcoin price started at \$7,200 in early 2020; on November 30, 2020, Bitcoin was trading for \$19,625, and the price reached around \$29,000 at the end of December 2020. The Bitcoin price increased by 14% in January 2021 and reached \$33,114. By

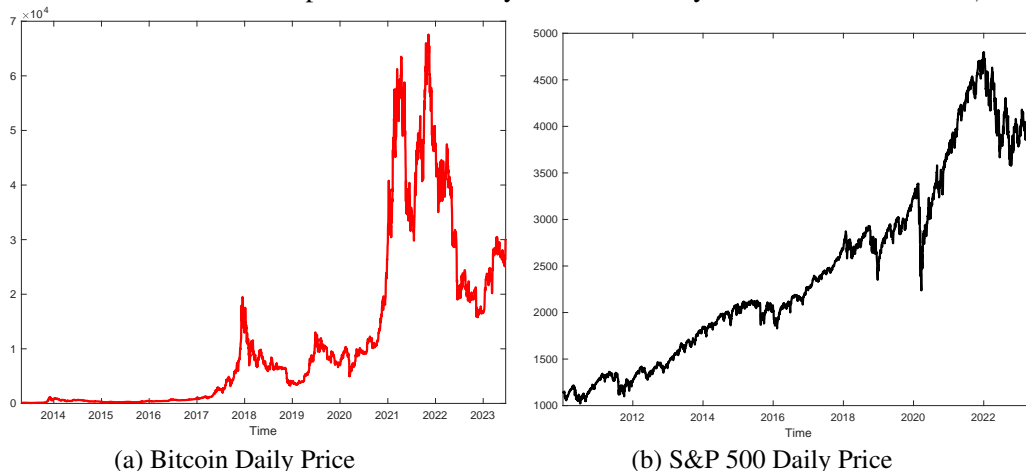


FIGURE 1. Daily Price

mid-April, Bitcoin prices reached the highest peak of \$63,503 on April 13, 2021 (second peak in

Fig 1a) before starting a decreasing process to reach \$29,807. On November 20, 2021, Bitcoin again achieved the highest value of \$65,995. In 2022, Bitcoin's price declined gradually, with prices only reaching \$19,784 at the end of June before falling further to \$16,547 at the end of December. In 2023, Bitcoin price increased gradually and reached the value of \$30,027 on June 21, 2023 (third peak in Fig 1a).

In Contrast to Bitcoin price, Fig 1b shows that S&P 500 index smooth out price fluctuations. The S&P 500 historical price used in Fig 1b starts on January 04, 2010, when S&P 500 index worth at \$1132. From 2010 to 2019, the U.S. economy was characterized by Stable economic growth and low-interest rates, which helped to keep equity prices on the rise. The S&P 500 index has steadily increased and almost tripled the index value from \$1132 to \$3230 on December 31, 2019. In early 2020, many countries issued quarantines in which businesses were ordered to shut down due to the global spread of COVID-19; the negative impact of such policy on the economy has sent the S&P 500 index into a tailspin, as shown in Fig 1b. In fact, on February 19, 2020, the S&P 500 closed at \$3,386, which was the highest value at that time. By March 23, 2020, the index plummeted to \$2,237, losing 34% of its value. The S&P 500 recovered the loss and continued a positive trend into 2021, reaching a peak of \$4726 on January 12, 2022. The index started a decreasing process and fell at the lower value of \$3577 on October 12, 2022, before increasing slightly to \$4409 on June 16, 2023.

2.2 Bitcoin and S&P 500 Index volatility over time.

The volatility of bitcoin and the stock market index (S&P 500) are produced and analyzed. The realized volatility measures the magnitude of daily price movements, regardless of direction, of some underlying, over a specific period. The realized volatility formula is provided in (4.1) with T =month for the short term and T =year for the long term. Let the number of observations m , and the daily observed price S_j on day t_j with $j = 1, \dots, m$. We have the following equations.

$$y_j = \log(S_j/S_{j-1}) \quad j = 2, \dots, m \quad \sigma_k^2 = \frac{252}{T} \sum_{j=0}^T y_{k-j}^2 \quad k = T, \dots, m \quad (2.1)$$

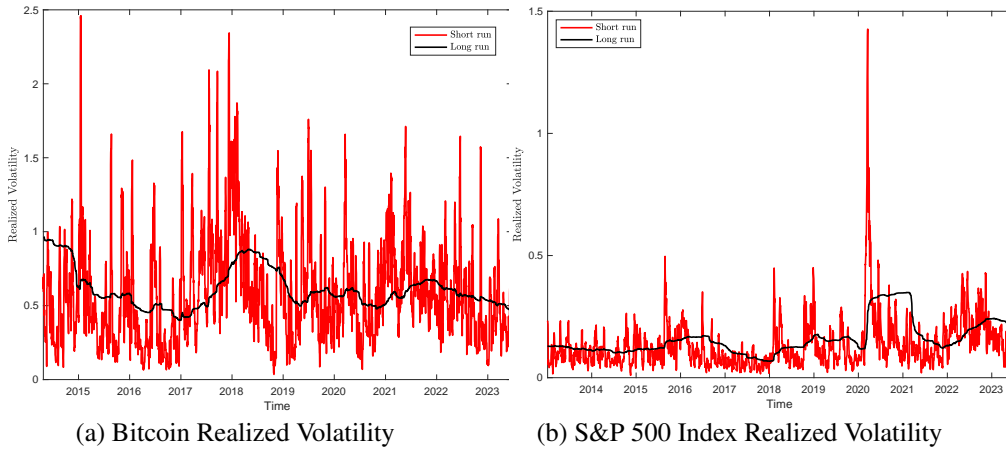


FIGURE 2. Realized Volatility

The volatility represents both risk and opportunity for financial investments. Fig (2a) shows that Bitcoin is a highly volatile asset, and the volatility persists over time. The highly volatile security quickly hits new highs and lows and has rapid growths and sharp falls. In contrast, the S&P 500 index is a lowly volatility asset. It has relatively stable price dynamics in the long run, as shown in Fig(2b). According to statistics used in Fig (2), on average, Bitcoin is almost five times more volatile than the S&P 500 index in the short run but four times more volatile in the long run.

3. GENERALIZED TEMPERED STABLE (GTS) PROCESS: OVERVIEW

The Lévy measure of the Generalized Tempered Stable (GTS) distribution ($V(dx)$) is defined (3.3) as a product of a tempering function ($q(x)$) (3.1) and a Lévy measure of the α -stable distribution ($V_{stable}(dx)$)(3.2).

$$q(x) = e^{-\lambda_+ x} \mathbf{1}_{x>0} + e^{-\lambda_- |x|} \mathbf{1}_{x<0} \quad (3.1)$$

$$V_{stable}(dx) = \left(\frac{\alpha_+}{x^{1+\beta_+}} \mathbf{1}_{x>0} + \frac{\alpha_-}{|x|^{1+\beta_-}} \mathbf{1}_{x<0} \right) dx \quad (3.2)$$

$$V(dx) = q(x)V_{stable}(dx) = \left(\frac{\alpha_+ e^{-\lambda_+ x}}{x^{1+\beta_+}} \mathbf{1}_{x>0} + \frac{\alpha_- e^{-\lambda_- |x|}}{|x|^{1+\beta_-}} \mathbf{1}_{x<0} \right) dx \quad (3.3)$$

where $0 \leq \beta_+ \leq 1$, $0 \leq \beta_- \leq 1$, $\alpha_+ \geq 0$, $\alpha_- \geq 0$, $\lambda_+ \geq 0$ and $\lambda_- \geq 0$.

The six parameters that appear have important interpretations. β_+ and β_- are the indexes of stability bounded below by 0 and above by 2 [20]. They capture the peakedness of the distribution similarly to the β -stable distribution, but the distribution tails are tempered. If β increases (decreases), then the peakedness decreases (increases). α_+ and α_- are the scale parameters, also called the process intensity [21]; they determine the arrival rate of jumps for a given size. λ_+ and λ_- control the decay rate on the positive and negative tails. Additionally, λ_+ and λ_- are also skewness parameters. If $\lambda_+ > \lambda_-$ ($\lambda_+ < \lambda_-$), then the distribution is skewed to the left (right), and if $\lambda_+ = \lambda_-$, then it is symmetric [22]. α and λ are related to the degree of peakedness and thickness of the distribution. If α increases (decreases), the peakedness and the thickness decrease (increase). Similarly, If λ increases (decreases), then the peakedness increases (decreases) and the thickness decreases (increases) [23].

The GTS distribution can be denoted by $X \sim GTS(\beta_+, \beta_-, \alpha_+, \alpha_-, \lambda_+, \lambda_-)$ and $X = X_+ - X_-$ with $X_+ \geq 0$, $X_- \geq 0$. $X_+ \sim TS(\beta_+, \alpha_+, \lambda_+)$ and $X_- \sim TS(\beta_-, \alpha_-, \lambda_-)$.

$$\int_{-\infty}^{+\infty} V(dx) = \begin{cases} +\infty & \text{if } \beta_+ \geq 0 \vee \beta_- \geq 0 \\ \alpha_+ \lambda_+^{\beta_+} \Gamma(-\beta_+) + \alpha_- \lambda_-^{\beta_-} \Gamma(-\beta_-) & \text{if } \beta_+ < 0 \wedge \beta_- < 0 \end{cases} \quad (3.4)$$

From (3.4), it results that when $\beta_+ < 0$, $TS(\beta_+, \alpha_+, \lambda_+)$ is of finite activity and can be written as a Compound Poisson process on the right side (X_+). we have similar pattern when $\beta_- < 0$. However, when $0 \leq \beta_+ \leq 1$, X_+ is an infinite activity process with infinite jumps in any given time interval. We have a similar pattern when $0 \leq \beta_- \leq 1$. In addition to the infinite activities process, we have

$$\int_{-\infty}^{+\infty} \min(1, |x|) V(dx) < +\infty \quad (3.5)$$

By adding the location parameter, the GTS distribution becomes $GTS(\mu, \beta_+, \beta_-, \alpha_+, \alpha_-, \lambda_+, \lambda_-)$ and we have:

$$Y = \mu + X = \mu + X_+ - X_- \quad Y \sim GTS(\mu, \beta_+, \beta_-, \alpha_+, \alpha_-, \lambda_+, \lambda_-) \quad (3.6)$$

Theorem 3.1

Consider a variable $Y \sim GTS(\mu, \beta_+, \beta_-, \alpha_+, \alpha_-, \lambda_+, \lambda_-)$, the characteristic exponent can be written

$$\Psi(\xi) = \mu \xi i + \alpha_+ \Gamma(-\beta_+) \left((\lambda_+ - i\xi)^{\beta_+} - \lambda_+^{\beta_+} \right) + \alpha_- \Gamma(-\beta_-) \left((\lambda_- + i\xi)^{\beta_-} - \lambda_-^{\beta_-} \right) \quad (3.7)$$

See [24] for theorem 3.1 proof

Theorem 3.2 (Cumulants κ_k)

Consider a variable $Y \sim GTS(\mu, \beta_+, \beta_-, \alpha_+, \alpha_-, \lambda_+, \lambda_-)$. The cumulants κ_k of the Generalized Tempered Stable distribution are defined as follows.

$$\kappa_1 = \mu + \alpha_+ \frac{\Gamma(1 - \beta_+)}{\lambda_+^{1 - \beta_+}} - \alpha_- \frac{\Gamma(1 - \beta_-)}{\lambda_-^{1 - \beta_-}} \quad \kappa_k = \alpha_+ \frac{\Gamma(k - \beta_+)}{\lambda_+^{k - \beta_+}} + (-1)^k \alpha_- \frac{\Gamma(k - \beta_-)}{\lambda_-^{k - \beta_-}} \quad (3.8)$$

See [24] for theorem 3.2 proof

The characteristic function, Fourier Transform ($F(f)$) and density function (f) of the GTS process Y can be written as follows

$$F[f](\xi) = e^{\Psi(-\xi)} \quad f(y) = \frac{1}{2\pi} \int_{-\infty}^{+\infty} e^{iyx} F[f](x) dx \quad (3.9)$$

Given the parameters $V = (\mu, \beta_+, \beta_-, \alpha_+, \alpha_-, \lambda_+, \lambda_-)$, we have the first and second order derivative of the function can be deduced from equation (3.10).

$$\frac{df(y)}{dV_j} = \frac{1}{2\pi} \int_{-\infty}^{+\infty} e^{iyx} \frac{dF(x)}{dV_j} dx \quad \frac{d^2 f(y)}{dV_k dV_j} = \frac{1}{2\pi} \int_{-\infty}^{+\infty} e^{iyx} \frac{d^2 F(x)}{dV_k dV_j} dx \quad (3.10)$$

4. METHODOLOGY: REVIEW OF ADVANCED FRFT - BASED SCHEME

4.1 Fast Fourier Transform and Fractional Fourier Transform .

The Conventional fast Fourier transform (FFT) algorithm is widely used to compute discrete convolutions, discrete Fourier transforms (DFT) of sparse sequences, and to perform high-resolution trigonometric interpolation [25]. The discrete Fourier transforms (DFT) are based on n -th roots of unity $e^{-\frac{2\pi i}{n}}$. The generalization of DFT is the fractional Fourier transform, which is based on fractional roots of unity $e^{-2\pi i \alpha}$, where α is an arbitrary complex number.

The fractional Fourier transform is defined on m -long sequence (x_1, x_2, \dots, x_m) as follows

$$G_{k+s}(x, \delta) = \sum_{j=0}^{m-1} x_j e^{-2\pi i j(k+s)\delta} \quad 0 \leq k < m \text{ \& } 0 \leq s \leq 1 \quad (4.1)$$

Let us have $2j(k+s) = j^2 + (k+s)^2 - (k-j+s)^2$, equation (4.1) becomes

$$\begin{aligned} G_{k+s}(x, \delta) &= \sum_{j=0}^{m-1} x_j e^{-\pi i(j^2 + (k+s)^2 - (k-j+s)^2)\delta} = e^{-\pi i(k+s)^2} \sum_{j=0}^{m-1} x_j e^{-\pi i j^2 \delta} e^{\pi i(k-j+s)^2 \delta} \\ &= e^{-\pi i(k+s)^2} \sum_{j=0}^{m-1} y_j z_{k-j} \quad y_j = x_j e^{-\pi i j^2 \delta} \ \& \ z_j = e^{\pi i(j+s)^2 \delta} \end{aligned} \quad (4.2)$$

The expression $\sum_{j=0}^{m-1} y_j z_{k-j}$ is a discrete convolution. Still, we need a circular convolution (i.e., $z_{k-j} = z_{k-j+m}$) to evaluate $G_{k+s}(x, \delta)$. The conversion from discrete convolution to discrete circular convolution is possible by extending the sequences y and z to length $2m$ defined as follows.

$$\begin{aligned} y_j &= e^{-2\pi i j^2 \delta} & z_j &= e^{-2\pi i(j+s)^2 \delta} & 0 \leq k < m \\ y_j &= 0 & z_j &= e^{-2\pi i(j+s-2m)^2 \delta} & m \leq k < 2m \end{aligned} \quad (4.3)$$

Taking into account the $2m$ -long sequence, the previous fractional Fourier transform becomes

$$G_{k+s}(x, \delta) = e^{-\pi i(k+s)^2} \sum_{j=0}^{2m-1} y_j z_{k-j} = e^{-\pi i(k+s)^2} DFT_k^{-1}[DFT_j(y) DFT_j(z)] \quad (4.4)$$

This procedure is referred to in the literature [25] as the Fast fractional Fourier Transform Algorithm with a total computational cost of $20m \log_2 m + 44m$ operations.

4.2 Fast Fourier Transform Algorithm and Direct Integration Methods.

We assume that $\mathcal{F}[f](y)$ is zero outside the interval $[-\frac{a}{2}, \frac{a}{2}]$; $\beta = \frac{a}{m}$ is the step size of the m input values of $\mathcal{F}[f](y)$, defined by $y_j = (j - \frac{m}{2})\beta$ for $0 \leq j < m$. Similarly, γ is the step size of the m output values of $f(t)$, defined by $x_k = (k - \frac{m}{2})\gamma$ for $0 \leq k < m$. By choosing the step size β on the input side and the step size γ in the output side, we fix the FRFT parameter $\delta = \frac{\beta\gamma}{2\pi}$ and yield [26] the density function f (3.10) at x_k .

$$\hat{f}(x_{k+s}) = \frac{\gamma}{2\pi} e^{-\pi i(k+s-\frac{n}{2})n\delta} G_{k+s}(\mathcal{F}[f](y_j) e^{-\pi i j n \delta}, -\delta) \quad 0 \leq s < 1 \quad (4.5)$$

The numerical integration of functions is another method to evaluate the inverse Fourier integrals called the Direct Integration Method. One of the sophisticated procedures is the Newton–Cotes quadrature rules, where the interval is approximated by some interpolating polynomials, usually in Lagrange form. The 12-point rule Composite Newton-Cotes Quadrature can be implemented and provides greater accuracy. The error analysis shows that the global error $O(h^{13})$ [27–29].

We assume $Q = 12$ and $m = Qn$; $\beta = \frac{a}{m}$ is the step size of the m input values $\mathcal{F}[f](y)$, defined by $y_{j+Qp} = (Qp + j - \frac{m}{2})\beta$ for $0 \leq p < n$ and $0 \leq j < Q$. Similarly, the output values of $f(x)$ is defined by $x_{Ql+f+s} = (Ql + f + s - \frac{m}{2})\gamma$ for $0 \leq l < n$, $0 \leq f < Q$ and $0 \leq s \leq 1$.

$$\hat{f}(x_{Ql+f+s}) = \beta \sum_{p=0}^{n-1} \sum_{j=0}^{Q-1} W_j e^{i(y_{j+Qp} x_{Ql+f+s})} F[f](y_{j+Qp}) \quad (4.6)$$

The weight value $\{W_j\}_{0 \leq j \leq Q}$ and details regarding the methodology are developed in [27–29].

4.3 Advanced Fast Fourier Transform (FRFT) Algorithm.

The Advanced Fast Fourier Transform (FRFT) algorithm combines the Fast Fractional Fourier Transform (FRFT) algorithm (4.5) and the 12-point rule Composite Newton-Cotes Quadrature (4.6) to evaluate the inverse Fourier integrals.

We assume that $\mathcal{F}[f](x)$ is zero outside the interval $[-\frac{a}{2}, \frac{a}{2}]$, $Q = 12$, $m = Qn$ and $\beta = \frac{a}{m}$ is the step size of the m input values $\mathcal{F}[f](y)$, defined by $y_{j+Qp} = (Qp + j - \frac{m}{2})\beta$ for $0 \leq p < n$ and $0 \leq j < Q$. Similarly, the output values of $f(x)$ is defined by $x_{Ql+f+s} = (Ql + f + s - \frac{m}{2})\gamma$ for $0 \leq l < n$, $0 \leq f < Q$ and $0 \leq s \leq 1$.

$$\begin{aligned} f(x_{Ql+f+s}) &= \frac{1}{2\pi} \int_{-\infty}^{+\infty} e^{iyx_{Ql+f+s}} F[f](y) dy = \frac{1}{2\pi} \int_{-a/2}^{a/2} e^{iyx_{Ql+f+s}} F[f](y) dy \\ &= \frac{1}{2\pi} \sum_{p=0}^{n-1} \int_{y_{Qp}}^{y_{Qp+Q}} e^{iyx_{Ql+f+s}} F[f](y) dy \quad (\text{composite rule}) \end{aligned} \quad (4.7)$$

Based on the Lagrange interpolating integration over $[x_{Qp}, x_{Qp+Q}]$ [27,28], we have the following expression.

$$\int_{x_{Qp}}^{x_{Qp+Q}} e^{iyx_{Ql+f+s}} F[f](x) dx \approx \beta \sum_{j=0}^{Q-1} w_j e^{iyx_{Ql+f+s}} F[f](x_{j+Qp}) \quad (4.8)$$

we consider $\widehat{f}(x_{Ql+f+s})$ the approximation of $f(x_{Ql+f+s})$. It results that the expression (4.7) becomes

$$\begin{aligned} \widehat{f}(x_{Ql+f+s}) &= \frac{\beta}{2\pi} \sum_{p=0}^{n-1} \sum_{j=0}^{Q-1} w_j F[f](y_{j+Qp}) e^{ix_{Ql+f+s} y_{j+Qp}} \\ &= \frac{\beta}{2\pi} \sum_{j=0}^{Q-1} w_j \sum_{p=0}^{n-1} F[f](y_{j+Qp}) e^{2\pi i \delta (Ql+f+s-\frac{m}{2})(Qp+j-\frac{m}{2})} \quad \beta\gamma = 2\pi\delta \quad (4.9) \\ &= \frac{\beta}{2\pi} e^{-\pi i \delta m (Ql+f+s-\frac{m}{2})} \sum_{j=0}^{Q-1} w_j G_{l+\frac{f+s}{Q}}(\xi_p, \delta Q^2) e^{2\pi i \delta (Ql-\frac{m}{2})j} e^{2\pi i \delta (f+s)j} \end{aligned}$$

We have the first fast fractional Fourier transform (FRFT) to perform on $\{\xi_p\}_{0 \leq p < n}$

$$G_{l+\frac{f+s}{Q}}(\xi_p, -\delta Q^2) = \sum_{p=0}^{n-1} y_p e^{-2\pi i (l+\frac{f+s}{Q})p\delta Q^2} \quad \xi_p = e^{-\pi i m p Q \delta} F[f](y_{j+Qp}) \quad (4.10)$$

$$\begin{aligned} \widehat{f}(x_{Ql+f+s}) &= \frac{\beta}{2\pi} e^{-\pi i \delta m (Ql+f+s-\frac{m}{2})} \sum_{j=0}^{Q-1} w_j G_{l+\frac{f+s}{Q}}(\xi_p, \delta Q^2) e^{2\pi i \delta (Ql-\frac{m}{2})j} e^{2\pi i \delta (f+s)j} \\ &= \frac{\beta}{2\pi} e^{-\pi i \delta m (Ql+f+s-\frac{m}{2})} G_{f+s}(z_j, \delta) \end{aligned} \quad (4.11)$$

We have the second fast fractional Fourier transform (FRFT) to perform on $\{z_j\}_{0 \leq j < Q}$

$$G_{f+s}(z_j, -\delta) = \sum_{j=0}^{Q-1} z_j e^{-2\pi i \delta (f+s)j} \quad z_j = w_j G_{l+\frac{f+s}{Q}}(y_p, \delta Q^2) e^{2\pi i \delta (Ql-\frac{m}{2})j} \quad (4.12)$$

The advanced FRFT - scheme yields the following approximation

$$\widehat{f}(x_{Ql+f+s}) = \frac{\beta}{2\pi} e^{-\pi i \delta m(Ql+f+s-\frac{m}{2})} G_{f+s}(z_j, \delta) \quad (4.13)$$

5. FITTING GENERAL TEMPERED STABLE DISTRIBUTION RESULTS

5.1 Review of the Maximum Likelihood Method.

From a probability density function $f(x, V)$ with parameter V of size $p = 7$ and the sample data X of size m , we define the Likelihood function and its derivatives as follows:

$$L(x, V) = \prod_{j=1}^m f(x_j, V) \quad l(x, V) = \sum_{j=1}^m \log(f(x_j, V)) \quad (5.1)$$

$$\frac{dl(x, V)}{dV_j} = \sum_{i=1}^m \frac{\frac{df(x_i, V)}{dV_j}}{f(x_i, V)} \quad \frac{d^2l(x, V)}{dV_k dV_j} = \sum_{i=1}^m \left(\frac{\frac{d^2f(x_i, V)}{dV_k dV_j}}{f(x_i, V)} - \frac{\frac{df(x_i, V)}{dV_k}}{f(x_i, V)} \frac{\frac{df(x_i, V)}{dV_j}}{f(x_i, V)} \right) \quad (5.2)$$

To perform the Maximum of the likelihood function (5.1), the quantities $\frac{df(x, V)}{dV_j}$ and $\frac{d^2f(x, V)}{dV_k dV_j}$ in (5.2) are the first and second order derivatives of the probability density and should be computed with high accuracy. The quantities $\frac{d^2l(x, V)}{dV_k dV_j}$ are critical in computing the Hessian Matrix and the Fisher Information Matrix.

Given the parameter $V = (\mu, \beta_+, \beta_-, \alpha_+, \alpha_-, \lambda_+, \lambda_-)$ and the sample data set X , we derive from (5.2) the following vector and matrix (5.3).

$$I'(X, V) = \left(\frac{dl(x, V)}{dV_j} \right)_{1 \leq j \leq p} \quad I''(X, V) = \left(\frac{d^2l(x, V)}{dV_k dV_j} \right)_{\substack{1 \leq k \leq p \\ 1 \leq j \leq p}} \quad (5.3)$$

The advanced FRFT - scheme developed previously is used to compute the likelihood function (5.1) and its derivatives (5.3) in the optimization process.

The local solution V^0 should meet the following requirements.

$$I'(x, V^0) = 0 \quad U^T I''(\mathbf{X}, \mathbf{V}^0) U \leq 0 \quad \forall U \in \mathbb{R}^p \quad (5.4)$$

The inequality in (5.4) is met when $I''(x, V^0)$ is a negative semi-definite matrix.

The Newton-Raphson Iteration Algorithm provides the numerical solution (5.5).

$$V^{n+1} = V^n - (I''(x, V^n))^{-1} I'(x, V^n) \quad (5.5)$$

See [30] for details on Maximum likelihood and Newton-Raphson Iteration procedure.

5.2 GTS Parameter Estimation from S&P 500 index.

The results of the GTS Parameter Estimation from S&P 500 return data are reported in Table 1. As expected, the stability indexes (β_-, β_+), the process intensities (α_-, α_+), and the decay rate (λ_-, λ_+) are all positive. In addition, the results show $0 \leq \beta_+ \leq 1$ and $0 \leq \beta_- \leq 1$; therefore, the positive S&P 500 rate of return (X_+) and the negative S&P 500 rate of return (X_-) are infinite activity processes, which means processes with an infinite number of jumps in any given time interval.

TABLE 1. FRFT Maximum Likelihood GTS Parameter Estimation

Model	μ	β_+	β_-	α_+	α_-	λ_+	λ_-
GTS	-0.693477	0.682290	0.242579	0.458582	0.414443	0.822222	0.727607

As shown in Table 1, We have $\alpha_- \leq \alpha_+$ and the higher arrival rate of jump on the right side contributes to the increasing global trend of the S&P 500 daily price in Fig 1b. Regarding the skewness parameters, we have $\lambda_- \leq \lambda_+$ and the S&P 500 return is a bit left-skewed distribution. The parameter analysis shows that the tail distribution is thicker on the negative side of the S&P 500 return distribution (X_-) than on the positive side of the distribution.

The implementation of the maximum likelihood method (in 5.1) was made possible by the numerical computations of the GTS probability density function $f(x, V)$ and its first and second derivative functions by the advanced FRFT - scheme developed previously in section 4. The results of the iteration process are reported in Table 2. each raw has eleven columns made of the iteration number, the seven parameters $\mu, \beta_+, \beta_-, \alpha_+, \alpha_-, \lambda_+, \lambda_-$ and three statistical indicators $\text{Log}(ML)$, $\|\frac{d\text{Log}(ML)}{dV}\|$, MaxEigenValue . The statistical indicators aim at checking if the two necessary and sufficient conditions described in equations(5.4) are all met. For each iteration in Table 2, $\text{Log}(ML)$ displays the value of the Naperian logarithm of the likelihood function $L(x, V)$ as described in (5.1); $\|\frac{d\text{Log}(ML)}{dV}\|$ displays the value of the norm of the first derivatives ($\frac{dl(x, V)}{dV_j}$) described in equations (5.2); and MaxEigenValue displays the maximum value of the seven Eigenvalues generated by the Hessian Matrix ($\frac{d^2l(x, V)}{dV_k dV_j}$) as described in equations (5.3).

The Newton-Raphson Iteration Algorithm (5.5) was implemented, and the results are reported in Table 2. As shown in Table 2, the log-likelihood ($\text{Log}(ML)$) value starts at -4664.7647 and increases to a limit of -4659.1914 ; the $\|\frac{d\text{Log}(ML)}{dV}\|$ value starts at 289.206866 to decreases to 0; and the maximum value of the Eigenvalues (MaxEigenValue) start at 48.3287566 and converge to -1.4542632 , which is negative. At the convergent solution, the Hessian matrix in (5.3) is a negative semi-definite matrix; both conditions in (5.4) are met, and we have a locally optimal solution.

TABLE 2. GTS Parameter Estimations from S&P 500 index

Iterations	μ	β_+	β_-	α_+	α_-	λ_+	λ_-	Log(ML)	$\ \frac{dLog(ML)}{dV}\ $	MaxEigenValue
1	-0.5266543	0.67666185	0.43662658	0.43109407	0.32587754	0.85012595	0.60145985	-4664.7647	289.206866	48.3287566
2	-0.5459715	0.67059496	0.42415971	0.44989796	0.34810329	0.80921924	0.60289955	-4660.2156	35.9853332	-6.0431046
3	-0.7108484	0.66676659	0.20613817	0.46963149	0.41246296	0.8368645	0.73679498	-4663.5777	1082.00304	449.252496
4	-0.6704327	0.66891111	0.11250993	0.46528242	0.50028087	0.83422813	0.86330646	-4660.5268	135.684998	15.1103621
5	-0.739816	0.66779246	0.09097181	0.48302677	0.45922815	0.85551132	0.81320574	-4660.0208	45.7082317	10.8419307
6	-0.6517205	0.65580459	0.19673172	0.47996977	0.42743878	0.85248358	0.75350741	-4659.833	46.3329967	11.8534517
7	-0.8136505	0.71997129	0.21558026	0.44023152	0.41952419	0.79423596	0.74025892	-4662.4815	1187.98211	166.006596
8	-0.7805857	0.70635344	0.22952102	0.44666893	0.41666063	0.80360771	0.7334486	-4659.7758	85.6584355	-3.4305336
9	-0.7543747	0.69912144	0.23468747	0.45029318	0.41542774	0.80935861	0.73077041	-4659.1944	1.07446211	-0.7993855
10	-0.7533784	0.69885561	0.23480071	0.45042677	0.41541378	0.80956671	0.73072468	-4659.1943	1.03706137	-0.8136858
11	-0.752414	0.69859801	0.2349108	0.45055614	0.41540021	0.8097682	0.73068024	-4659.1942	1.00184387	-0.8273569
12	-0.7514794	0.69834808	0.23501796	0.45068156	0.41538701	0.80996353	0.73063702	-4659.1942	0.96860649	-0.8404525
13	-0.7496917	0.69786927	0.23522417	0.4509216	0.41536164	0.81033731	0.73055392	-4659.194	0.90739267	-0.8650984
14	-0.7471903	0.69719768	0.23551545	0.45125776	0.41532584	0.81086063	0.73043671	-4659.1938	0.82669598	-0.8987475
15	-0.7463993	0.69698491	0.23560822	0.45136413	0.41531445	0.8110262	0.73039942	-4659.1937	0.80232744	-0.9091961
16	-0.7456279	0.69677723	0.23569899	0.45146791	0.41530331	0.8111877	0.73036294	-4659.1937	0.77907591	-0.9193009
17	-0.7434222	0.69618233	0.23596025	0.45176484	0.41527126	0.81164974	0.73025805	-4659.1935	0.71530396	-0.9477492
18	-0.7427203	0.69599272	0.2360439	0.45185938	0.41526101	0.81179683	0.73022449	-4659.1934	0.69583386	-0.9566667
19	-0.7376152	0.69460887	0.23665992	0.45254797	0.41518555	0.81286777	0.72997772	-4659.193	0.56549166	-1.0197019
20	-0.7353516	0.69399264	0.23693733	0.45285383	0.41515159	0.81334323	0.72986678	-4659.1929	0.51375646	-1.0466686
21	-0.7342715	0.69369811	0.23707047	0.45299987	0.41513529	0.81357023	0.72981356	-4659.1928	0.47702329	-1.0633442
22	-0.727748	0.69191195	0.23788938	0.45388257	0.41503509	0.81494168	0.72948683	-4659.1924	0.30254549	-1.1564316
23	-0.7269375	0.69168915	0.23799284	0.45399234	0.41502243	0.81511217	0.72944561	-4659.1924	0.28659447	-1.1671214
24	-0.7261524	0.69147312	0.23809343	0.45409871	0.41501011	0.81527736	0.72940554	-4659.1923	0.27235218	-1.177299
25	-0.7074205	0.68625723	0.24059125	0.45665159	0.41470173	0.81923664	0.72841073	-4659.1916	0.15127988	-1.3705213
26	-0.7028887	0.68497607	0.24122265	0.45727561	0.4146222	0.82020261	0.72815815	-4659.1915	0.12096032	-1.4033087
27	-0.6987925	0.68381109	0.24180316	0.45784257	0.4145479	0.82107955	0.72792474	-4659.1914	0.07862954	-1.4283679
28	-0.6934505	0.68228736	0.24256739	0.45858391	0.41444901	0.82222574	0.72761631	-4659.1914	0.75324649	-1.6442249
29	-0.6934765	0.68229002	0.24257963	0.45858236	0.41444404	0.82222285	0.72760762	-4659.1914	9.93E-06	-1.4542674
30	-0.6934774	0.68229032	0.24257975	0.45858219	0.41444396	0.8222226	0.7276075	-4659.1914	7.4193E-08	-1.4542632

GTS Parameter Estimation (in Table 1) was used to compare the empirical values and theoretical values of the first derivative of the GTS probability density function. The comparison provides the degree of accuracy for the advanced FRFT scheme and the fitness between empirical and theoretical values. As shown in Fig 3, the empirical values $\left(\frac{df(x_i, V)}{dV_j}\right)_{\substack{1 \leq i \leq m \\ 1 \leq j \leq 7}}$ generated by S&P 500 returns are displayed in circles (red for the parameter positive sign and black for the parameter negative sign); and the theoretical values $\left(\frac{df(x, V)}{dV_j}\right)_{1 \leq j \leq 7}$ are displayed in a straight curve. As shown in Fig 3a and Fig 3c, β_+ and α_+ have a higher effect on the Probability density function (pdf) than β_- and α_- respectively. However, in Fig 3b, λ_- and λ_+ are symmetric and have the same effect on pdf.

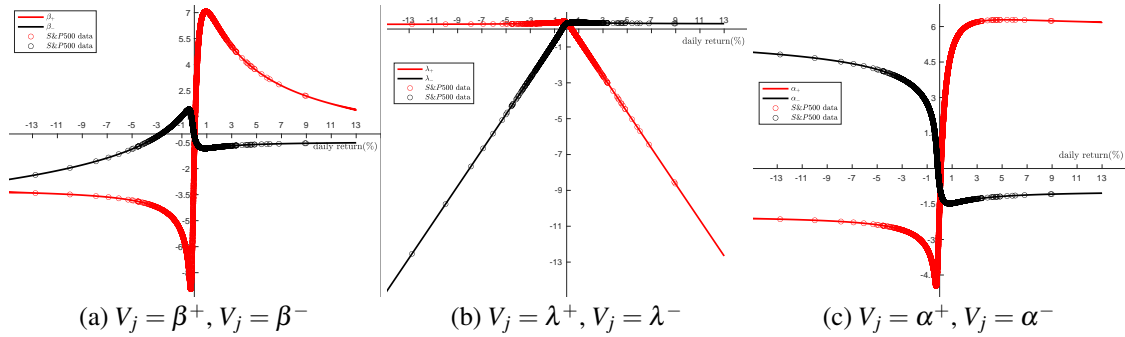


FIGURE 3. $\frac{df(x_i, V)}{dV_j}$

5.3 GTS Parameter Estimation: Bitcoin.

The results of the GTS Parameter Estimation from Bitcoin returns are reported in Table 3. As expected, the stability indexes (β_-, β_+), the process intensities (α_-, α_+), and the decay rate (λ_-, λ_+) are all positive. The results show $0 \leq \beta_+ \leq 1$ and $0 \leq \beta_- \leq 1$, the positive Bitcoin return (X_+) and the negative Bitcoin return (X_-) are infinite activity processes, which means each process has an infinite number of jumps in any given time interval.

TABLE 3. FRFT Maximum Likelihood GTS Parameter Estimation

Model	μ	β_+	β_-	α_+	α_-	λ_+	λ_-
GTS	-0.736924	0.461378	0.267178	0.810017	0.517347	0.215628	0.191937

As shown in Table 1, We have $\alpha_- \leq \alpha_+$ and the higher arrival rate of jump on the right side (X_+) contributes to the increasing global trend of the bitcoin daily price in Fig 1b. Regarding the skewness parameters, we have $\lambda_- \leq \lambda_+$ and the S&P 500 return is a bit left-skewed distribution. The parameter analysis shows that the tail distribution is thicker on the negative side of the Bitcoin return distribution (X_-) than on the positive side.

The Newton-Raphson Iteration Algorithm (5.5) was implemented, and the results are reported in Table 4. As shown in Table 4, the log-likelihood ($Log(ML)$) value starts at -10036.656 and increases to a limit of -9751.2193 ; the $\| \frac{dLog(ML)}{dV} \|$ value starts at 3188.1469 and decreases to almost 0; and the maximum value of the Eigenvalues ($MaxEigenValue$) start at 2854.2231 and converge to -0.000436 , which is negative. At the convergent solution, the Hessian matrix in (5.3) is a negative semi-definite matrix; both conditions in (5.4) are met, and we have a locally optimal solution.

TABLE 4. GTS Parameter Estimations from Bitcoin returns

Iterations	μ	β_+	β_-	α_+	α_-	λ_+	λ_-	$Log(ML)$	$\ \frac{dLog(ML)}{dV} \ $	$MaxEigenValue$
1	-0.5973	0.3837	0.4206	1.872	0.694	0.5333	0.219	-10036.656	3188.1469	2854.2231
2	-1.2052311	0.35850753	0.44451399	2.00512495	0.62313779	0.53840744	0.20635235	-9912.1541	1971.95236	1518.15345
3	-1.624469	0.31755508	0.45798507	2.23748588	0.58475918	0.56388213	0.17998332	-9865.5242	952.027546	716.347539
4	-1.9959515	0.2615866	0.47359748	2.57864607	0.5494987	0.60990478	0.16377681	-9862.2551	440.489423	295.233361
5	-2.8340545	-0.0033236	0.55268657	4.51611949	0.47359381	0.87264266	0.130233	-9911.337	510.396179	60.6518499
6	-2.701598	0.07378625	0.54127007	3.76512451	0.47819392	0.7743675	0.13294829	-9896.0802	611.613266	117.692562
7	-1.4130144	0.37715064	0.48510637	1.50024644	0.5523787	0.39998447	0.15474644	-9804.2548	801.962681	307.039536
8	-1.049984	0.45100489	0.4741659	1.13318569	0.56070768	0.30817133	0.15667085	-9775.871	728.753228	295.768229
9	-0.8211241	0.50542632	0.46591368	0.90824445	0.54487666	0.23555274	0.1533588	-9756.7912	397.102674	133.652433
10	-0.7319208	0.53998085	0.44372538	0.81377008	0.54717214	0.19930192	0.15902826	-9752.0888	89.8942291	12.4808028
11	-1.2317854	0.58475806	0.23780021	0.81260395	0.49719481	0.18597445	0.19343462	-9751.3131	32.1533364	-2.5188051
12	-0.7150133	0.4721273	0.29761245	0.80521805	0.52356611	0.21204916	0.18644449	-9750.6869	5.52013773	0.11490414
13	-0.7271098	0.45992936	0.27054512	0.80932883	0.51829775	0.21585683	0.19139837	-9751.2179	1.13726334	0.19172007
14	-0.7750442	0.46778988	0.25646086	0.81245021	0.51411912	0.21450942	0.19360685	-9751.2252	1.00910053	-0.9423667
15	-0.7090246	0.45678856	0.27535855	0.80819689	0.51977265	0.21641582	0.19065445	-9751.2151	0.68576109	0.57268124
16	-0.7494266	0.46338031	0.26341052	0.81084098	0.51624184	0.21529106	0.19253194	-9751.2211	0.65747338	-0.2888343
17	-0.7429071	0.46233754	0.26537785	0.8104111	0.51681851	0.21546689	0.19222166	-9751.2201	0.65058847	-0.1361475
18	-0.7401206	0.46189156	0.2662183	0.81022749	0.51706495	0.21554213	0.19208913	-9751.2197	0.64914609	-0.0724136
19	-0.7369888	0.4613886	0.26715947	0.81002148	0.51734136	0.21562718	0.19194083	-9751.2193	0.64887078	-0.0018685
20	-0.7369633	0.4613845	0.26716714	0.8100198	0.51734361	0.21562787	0.19193962	-9751.2193	0.64887314	-0.0012986
21	-0.7369455	0.46138165	0.26717247	0.81001863	0.51734517	0.21562835	0.19193878	-9751.2193	0.64887482	-0.0009025
22	-0.7369332	0.46137967	0.26717617	0.81001782	0.51734626	0.21562869	0.1919382	-9751.2193	0.64887601	-0.0006273
23	-0.7369246	0.46137829	0.26717875	0.81001726	0.51734702	0.21562892	0.19193779	-9751.2193	0.64887685	-0.000436

GTS parameter estimation (in Table 3) was used to compare the empirical values and theoretical values of the first derivative of the GTS probability density function. Similar to Fig 3, in Fig

4, the empirical values $\left(\frac{df(x_i, V)}{df(x_i, V)} \right)_{\substack{1 \leq i \leq m \\ 1 \leq j \leq 7}}$ generated by the Bitcoin returns are displayed in circles

(red for the parameter positive sign and black for the parameter negative sign; and the theoretical values $\left(\frac{df(x,V)}{dV_j}\right)_{1 \leq j \leq 7}$ are displayed in a straight curve. As shown in Fig 4a, β_- has a higher effect on the Probability density function (pdf) than β_+ , but α_+ has a higher effect than α_- in Fig 4c. However, in Fig 4b, λ_- and λ_+ are symmetric and have the same effect on pdf.

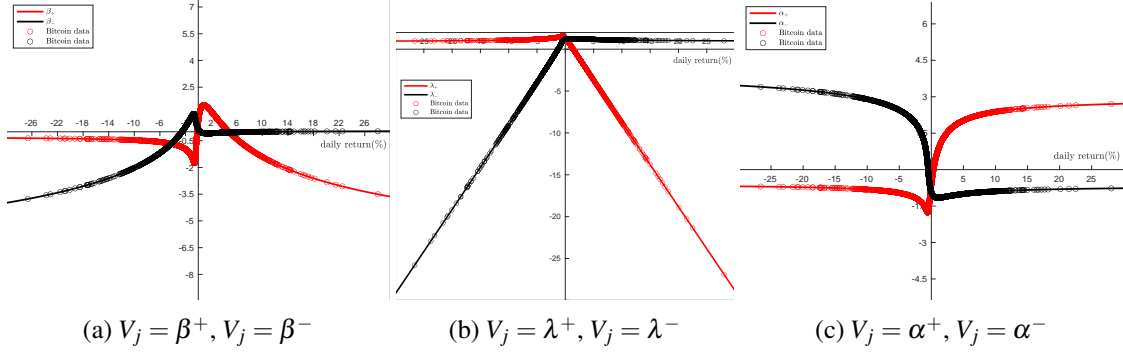


FIGURE 4. $\frac{df(x_i,V)}{dV_j}$

The difference in amplitude effect is more visible when Fig 3 (S&P 500 index) and Fig 4c (Bitcoin) are put together with each GST parameter side by side. As shown in the Appendix A.1, the stability indexes (β_-, β_+) and the process intensities (α_-, α_+) degenerated from S&P 500 index fitting have higher effects on the GST probability density function (pdf) whereas the decay rate (λ_-, λ_+) degenerated from Bitcoin fitting has higher effects on the GST probability density function (pdf).

6. ANALYSIS AND FINDINGS: DENSITY FUNCTION AND KEY STATISTICS

The GTS parameter estimates from S&P 500 return and Bitcoin return data are used to compute the GTS probability density functions, and their main characteristics are analyzed. As illustrated in Fig5, Both graphs show that tail events are much more prevalent than we would expect with a Normal distribution. The heavy-tailed distribution captures the huge price swings of the Bitcoin and S&P 500 index. According to Table 5, the theoretical Kurtosis statistics are 8.92319 for S&P 500 returns and 9.74633 for Bitcoin returns, which are almost three times the kurtosis of the Normal distribution. The peakedness of the density function is another characteristic, as shown in Fig5. In contrast to the Normal distribution, there is a higher concentration of data values around the mean. The degree of concentration is much higher for S&P 500 return in Fig5b than Bitcoin return distribution in Fig5a. Many studies show that Kurtosis is not a measure of peakedness but rather a measure of tailedness [31–33]. Both GTS distributions are called in the literature leptokurtic distributions.

For Bitcoin return distributions in Fig5a, the Normal probability density (red curve) with mean ($\kappa_1 = 0.15\%$) and standard deviation ($\sigma = 3.99\%$) is plotted alongside the GTS probability density (black curve). According to the Normal distribution, about 35.15% of Bitcoin returns (in the purple area) are within -1.57% and 2.07% , 19.63% lower than the actual percentage of Bitcoin returns. According to the GTS distribution, about 20.72% of Bitcoin returns (in the blue area)

are within -9.53% and -1.57% ; and on the right side, 20.99% of Bitcoin returns (in the yellow area) are within 2.07% and 10.05% . However, as shown in the red and blue areas in Fig5a, both percentages are overestimated by the normal distribution.

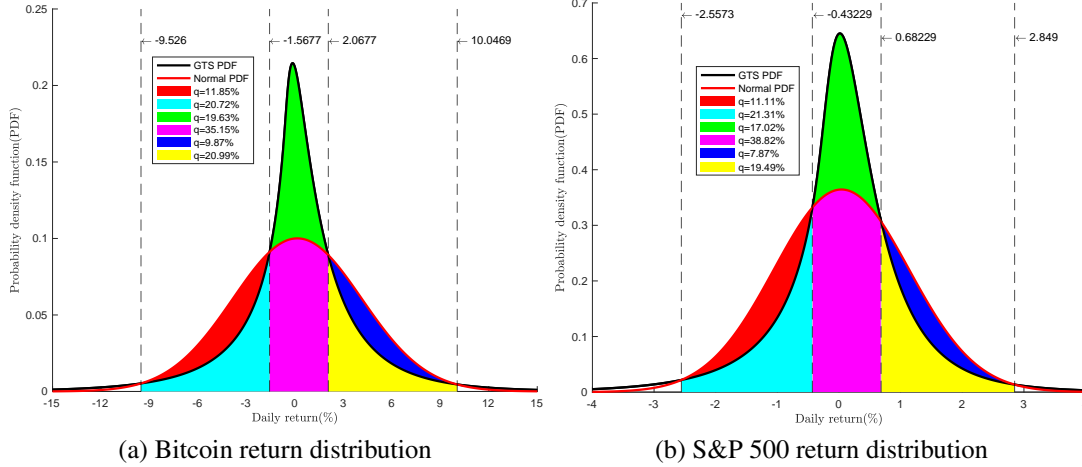


FIGURE 5. Probability density functions

For S&P 500 return distributions in Fig5b, the Normal probability density (red curve) with a mean ($\kappa_1 = 0.04\%$) and a standard deviation ($\sigma = 1.09\%$) is plotted along with the GTS probability density (black curve). Similar to the previous analysis, according to the Normal distribution, about 38.82% of S&P 500 index returns are concentrated within -0.43% and 0.68% ; the percentage is 17.02% lower than the actual percentage of S&P 500 returns. According to the GTS distribution, about 21.31% of S&P 500 (in cyan area) are within -2.56% and -0.43% ; and on the right side, 19.49% of S&P 500 returns (in yellow area) are within 0.68% and 2.85% . However, as shown in the red and blue areas in Fig5a, both percentages are overestimated by the normal distribution.

The GTS probability density functions from S&P 500 returns and Bitcoin returns are compared in Fig6. The heavy-tailedness is the main characteristic of the GTS probability density function, whereas the GTS probability density function from the S&P 500 index is characterized by peakedness.

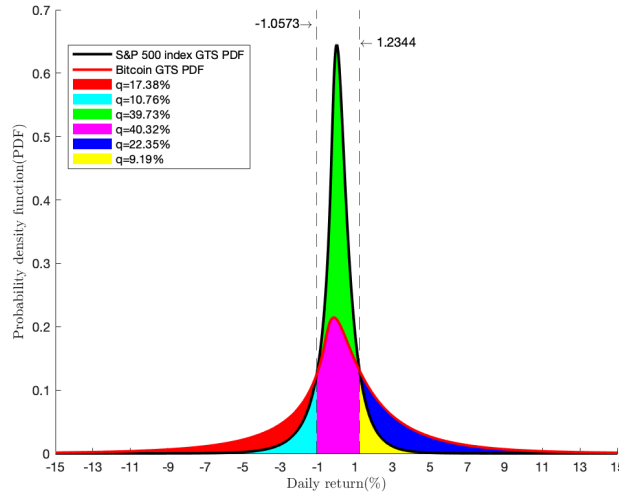


FIGURE 6. Bitcoin Versus S&P 500 returns

For Bitcoin return distribution in Fig6, about 40.32% of Bitcoin returns (in the purple area) are within -1.06% and 1.23% ; 28.14% of Bitcoin returns are less than -1.06% ; and 31.54% of Bitcoin returns are more than 1.23% . While S&P 500 return distribution records about 80.05% of S&P 500 return within -1.06% and 1.23% ; 10.76% of S&P 500 returns (in cyan area) are less than -1.06% ; and 9.19% of S&P 500 returns (in yellow area) are more than 1.23% .

Table 5 provides the empirical statistics from the sample data and the key statistics of GTS distribution. For S&P 500 index, the sample size was 3386 rate of returns with the largest and smallest values 8.96883% and -12.7652% respectively. For Bitcoin, the sample size was 3705 rate of returns with the largest and smallest values 28.0520% and -26.6197% , respectively.

TABLE 5. Summary Statistics

Label	S&P 500		Bitcoin	
	Empirical	Theoretical	Empirical	Theoretical
Sample size(m)	3386		3705	
Mean (κ_1)	0.0401%	0.0401%	0.1488%	0.1489%
Standard deviation (σ)	1.1192%	1.0947%	3.9784%	3.9866%
Coefficient of Variation (CV)	27.88917	27.27762	26.73285	26.77318
Skewness ($\frac{\kappa_3}{\sigma^{3/2}}$)	-0.72331	-0.57964	-0.32744	-0.31987
Kurtosis ($3 + \frac{\kappa_4}{\sigma^2}$)	16.04641	8.92319	8.88504	9.74633
Max value	8.9683%		28.0520%	
Min Value	-12.7652%		-26.6197%	

As shown in Table 5, the empirical and theoretical Mean (κ_1), Standard deviation (σ), and Coefficient of Variation (CV) are consistent for each asset. However, the empirical estimations overestimate the Kurtosis and skewness statistics, except for the S&P 500 index; the plausible explanation is the impact of the outliers (-12.7652% , 8.96883%).

7. ANALYSIS AND FINDINGS: VALUE-AT-RISK AND AVERAGE VALUE-AT-RISK

The value-at-risk (VaR) and average value-at-risk (AVaR) are widely used financial risk measures. The value at risk (VaR) can be defined as the minimum level of loss or profit at a given confidence level. The estimation of the value-at-risk (VaR) and average value-at-risk (AVaR) are compared to the empirical VaR and AVaR.

We consider the following sorted sample x_1, x_2, \dots, x_n corresponding to instant t_1, t_2, \dots, t_n , the empirical VaR and AVaR at tail probability (α) are obtained by applying the following estimators. [34, 35].

$$\widehat{VaR}_\alpha = x_{(\lceil n\alpha \rceil)} \quad \widehat{AVaR}_\alpha = \frac{1}{1-\alpha} \left[\frac{1}{n} \sum_{j=\lceil n\alpha \rceil+1}^n x_j + \left(\frac{\lceil n\alpha \rceil}{n} - \alpha \right) x_{(\lceil n\alpha \rceil)} \right] \quad (7.1)$$

Where the notation $\lceil x \rceil$ stands for the smallest integer larger than x .

7.1 Analysis and Findings: Value-at-Risk ($VaR_\alpha(X)$).

Based on the characteristic exponent of the GTS distribution, we develop a methodology to compute the theoretical value at risk (VaR). We assume the return distribution function is continuous; that is, there are no point masses. Formally, the VaR at confidence level $(1-\alpha)$ or tail probability (α) is the α^{th} quantile of the return distribution and has the following mathematical expression.

$$VaR_\alpha(X) = \inf\{x | p(X \leq x) \geq \alpha\} = F^{-1}(x) \quad (7.2)$$

Where $0 \leq \alpha \leq 1$ and F^{-1} is the inverse of the cumulative distribution function. The GTS($\mu, \beta_+, \beta_-, \alpha_+, \alpha_-, \lambda_+, \lambda_-$) density and cumulative functions do not have closed form, which makes it difficult estimate of the α^{th} quantile analytically. Therefore, we rely on the computational method based on the Advanced FRFT developed previously. We consider a sequence of GTS cumulative function values $(F_j)_{1 \leq j \leq m}$ on a sequence of input value $(x_j)_{1 \leq j \leq m}$. $(F_j)_{1 \leq j \leq m}$ is generated by the Advanced FRFT scheme. We also consider x_α the α^{th} quantile defined by $F(x_\alpha) = \alpha$ with $x_i < x_\alpha < x_{i+1}$ and $F_i < F(x_\alpha) < F_{i+1}$.

By applying the Taylor series approximation, we have :

$$F(x_\alpha) = F_i + \frac{u}{1!} F_i^{(1)} + \frac{u^2}{2!} F_i^{(2)} + \frac{u^3}{3!} F_i^{(3)} + \frac{u^4}{4!} F_i^{(4)} + O(u^4) \quad (7.3)$$

$$u = x_\alpha - x_i \quad \lim_{u \rightarrow 0} O(u^4) = 0$$

By applying the central difference representations of $O(\Delta^2)$ with $\Delta = x_{i+1} - x_i$, we have the values of first, second, third, and fourth-order derivatives.

$$a_1 = \Delta F_i^{(1)} = \frac{-F_{i-1} + F_{i+1}}{2} \quad a_3 = \Delta^3 F_i^{(3)} = \frac{-F_{i-2} + 2F_{i-1} - 2F_{i+1} + F_{i+2}}{2} \quad (7.4)$$

$$a_2 = \Delta^2 F_i^{(2)} = F_{i-1} - 2F_i + F_{i+1} \quad a_4 = \Delta^4 F_i^{(4)} = F_{i-2} - 4F_{i-1} + 6F_i - 4F_{i+1} + F_{i+2}$$

By removing the function $O(x_\alpha - x_i)$ in (7.3), we have the following polynomial equation:

$$-(\alpha - F_i) + a_1 \frac{x_\alpha - x_i}{x_{i+1} - x_i} + \frac{a_2}{2!} \left(\frac{x_\alpha - x_i}{x_{i+1} - x_i} \right)^2 + \frac{a_3}{3!} \left(\frac{x_\alpha - x_i}{x_{i+1} - x_i} \right)^3 + \frac{a_4}{4!} \left(\frac{x_\alpha - x_i}{x_{i+1} - x_i} \right)^4 = 0 \quad (7.5)$$

Let us take $b_0 = -(\alpha - F_i)$, $b_1 = a_1$, $b_2 = \frac{a_2}{2!}$, $b_3 = \frac{a_3}{3!}$, $b_4 = \frac{a_4}{4!}$ and $y = \frac{x_\alpha - x_i}{x_{i+1} - x_i}$. The polynomial equation becomes:

$$b_0 + b_1y + b_2y^2 + b_3y^3 + b_4y^4 = 0 \quad (7.6)$$

The Intermediate Value Theorem guarantees the existence of the solution (y) over the interval (0,1). For a root (y) of the equation (7.6) with $0 < y < 1$, we have the estimation of the α^{th} quantile as follows.

$$x_\alpha = x_i + y(x_{i+1} - x_i) \quad (7.7)$$

It was shown in Fig6 that the GTS distribution generated from Bitcoin and S&P500 returns are not symmetric. Therefore, for a given tail probability (α), the $VaR_\alpha(X)$ is not expected to yield the same value as the $VaR_{1-\alpha}(X)$ for a confident level ($1 - \alpha$). For tail probability (α) from 0.5%, 1%, ..., 10%, the theoretical and empirical Value-at-Risk ($VaR_\alpha(X)$) was computed and summarized in table 8 (appendix B.2). For the correspondent confidence level ($1 - \alpha$) from 90%, ..., 99%, 99.5% the estimations of the the theoretical and empirical Value-at-Risk ($VaR_{1-\alpha}(X)$) are summarised in table 6. Both tables show that the empirical and theoretical Value-at-Risk is consistent. As expected, the bitcoin theoretical and empirical Value-at-Risk ($VaR_{1-\alpha}(X)$) are higher than that of the S&P 500 index, which is consistent with the heavy-tailedness of the bitcoin return. We have the same pattern in table 8.

TABLE 6. Value-at-Risk Statistics

$VaR_{1-\alpha}(X)$	S&P 500 index (%)		Bitcoin (%)	
Confidence Level ($1 - \alpha$)	Empirical	Theoretical	Empirical	Theoretical
90%	1.1819	1.1760	4.3173	4.2392
91%	1.2638	1.2499	4.5631	4.5379
92%	1.3311	1.3333	4.8620	4.8761
93%	1.4050	1.4288	5.1729	5.2647
94%	1.4770	1.5402	5.5775	5.7202
95%	1.5939	1.6738	6.3628	6.2679
96%	1.7231	1.8399	7.1021	6.9508
97%	1.9259	2.0583	7.9802	7.8507
98%	2.2504	2.3738	9.5034	9.1534
99%	2.8115	2.9334	11.1161	11.4653
99.5%	3.3713	3.5166	13.5660	13.8771

As shown in table 6, The 95% $VaR_{1-\alpha}(X)$ of both S&P 500 index and Bitcoin are equal to 3.52% and 13.88% respectively. That is, Bitcoin gains more than 13.88% of its present value with a probability of 5%, whereas the S&P 500 index gains only more than 3.52% of its present value with a probability of 5%. As illustrated in Fig 8a and Fig 8b, the value-at-risk ($VaR_\alpha(X)$) of bitcoin and S&P 500 index increase at an increasing rate in each interval. There is also a discrepancy between the value-at-risk ($VaR_\alpha(X)$) of bitcoin and S&P 500 index. A disadvantage of value-at-risk (VaR) [35] is that it does not provide any information about the magnitude of the losses or profits larger than the value-at-risk level.

7.2 Analysis and Findings: Average Value-at-Risk ($AVaR_\alpha(X)$).

The average value-at-risk ($AVaR_\alpha$) at tail probability α is defined as the average of the value-at-risks (VaRs) that are larger than the value-at-risk (VaR) at tail probability α . The mathematical expression can be written as follows

$$AVaR_\alpha(X) = \frac{1}{\alpha} \int_0^\alpha VaR_y(X) dy \quad (7.8)$$

The Generalized Tempered Stable (GTS) distribution is a continuous variable (X), and the Value-at-Risk (VaR) has a simplified expression $VaR_\alpha(X) = F_X^{-1}(\alpha)$ in (7.2) and the integral in (7.8) becomes

$$\int_0^\alpha VaR_y(X) dy = \int_0^\alpha F_X^{-1}(y) dy = \int_0^{F_X^{-1}(\alpha)} \theta dF_X(\theta) = E[X \mathbb{1}_{\{X \leq VaR_\alpha(X)\}}] \quad (7.9)$$

The average value-at-risk (7.8) becomes

$$\begin{aligned} AVaR_\alpha(X) &= \frac{1}{\alpha} E[X \mathbb{1}_{\{X \leq VaR_\alpha(X)\}}] = \frac{1}{\alpha} E[VaR_\alpha(X) \mathbb{1}_{\{X \leq VaR_\alpha(X)\}} + (X - VaR_\alpha(X))^-] \\ &= VaR_\alpha(X) + \frac{1}{\alpha} E[(X - VaR_\alpha(X))^-] \end{aligned} \quad (7.10)$$

For the confident level $(1 - \alpha)$, the average value-at-risk ($AVaR_{1-\alpha}$) becomes

$$\begin{aligned} AVaR_{1-\alpha}(X) &= \frac{1}{1-\alpha} \int_0^{1-\alpha} VaR_{1-y}(X) dy = \frac{1}{1-\alpha} \int_\alpha^1 VaR_y(X) dy \\ &= VaR_{1-\alpha}(X) + \frac{1}{1-\alpha} E[(X - VaR_{1-\alpha}(X))^+] \end{aligned} \quad (7.11)$$

We have the following expression on the loss ($\alpha \leq \frac{1}{2}$) and the profit ($\alpha \geq \frac{1}{2}$) of the return distribution

$$\begin{aligned} AVaR_\alpha(X) &= VaR_\alpha(X) + \frac{1}{\alpha} E[(X - VaR_\alpha(X))^-] & \alpha < \frac{1}{2} \\ AVaR_{1-\alpha}(X) &= VaR_{1-\alpha}(X) + \frac{1}{1-\alpha} E[(X - VaR_{1-\alpha}(X))^+] & \alpha > \frac{1}{2} \end{aligned} \quad (7.12)$$

Theorem 7.1

Let $k \in \mathbb{R}$. X is a GTS($\mu, \beta_+, \beta_-, \alpha_+, \alpha_-, \lambda_+, \lambda_-$) random variable with characteristic exponent function $\Psi(\xi)$.

There exists $q > 0$ such that

$$\begin{aligned} E[(X - k)^+] &= \frac{1}{2\pi} \int_{-\infty+iq}^{+\infty+iq} \frac{-1}{z^2} e^{izk + \Psi(-z)} dz \\ E[(X - k)^-] &= \frac{1}{2\pi} \int_{-\infty-iq}^{+\infty-iq} \frac{1}{z^2} e^{izk + \Psi(-z)} dz \end{aligned} \quad (7.13)$$

Proof:

$g(X, k) = (X - k)^+$ is the payoff of the call option, and the Fourier transform of g is derived as

follows:

$$\begin{aligned}\mathcal{F}[g](y, k) &= \int_{-\infty}^{+\infty} e^{-iyx} g(x, k) dx = \int_{-\infty}^{+\infty} e^{-iyx} (x-k)^+ dx = \int_k^{+\infty} e^{-iyx} (x-k) dx \\ &= \left[\frac{1 + (x-k)iy}{y^2} e^{-iyx} \right]_k^{+\infty} = -\frac{1}{y^2} e^{-iyk} \quad \text{for } \Im(y) < 0\end{aligned}\quad (7.14)$$

Where $\Im(y)$ is the imaginary of y .

If the payoff function becomes the payoff of the put option, we have $g(X, k) = (X - k)^-$ and the Fourier transform becomes

$$\mathcal{F}[g](y, k) = \left[\frac{1 + (x-k)iy}{y^2} e^{-iyx} \right]_{-\infty}^k = \frac{1}{y^2} e^{-iyk} \quad \text{for } \Im(y) > 0 \quad (7.15)$$

The call payoff (7.13) can be recovered from the inverse of Fourier if there exists $q > 0$ such that

$$\check{g}(x, k) = \frac{1}{2\pi} \int_{-\infty+iq}^{+\infty+iq} e^{iyx} \mathcal{F}[g](y, k) dy = -\frac{1}{2\pi} \int_{-\infty+iq}^{+\infty+iq} \frac{1}{y^2} e^{iy(x-k)} dy \quad (7.16)$$

$$\begin{aligned}E[(X - k)^+] &= \int_{-\infty}^{+\infty} g(y, k) f(y) dy = \frac{1}{2\pi} \int_{-\infty}^{+\infty} \int_{-\infty}^{+\infty} e^{-iyz + \Psi(z)} g(y, k) dy dz \quad g(y, k) = (y - k)^+ \\ &= \frac{1}{2\pi} \int_{-\infty}^{+\infty} e^{\Psi(z)} \int_{-\infty}^{+\infty} e^{-iyz} g(y, k) dy dz = \frac{1}{2\pi} \int_{-\infty-iq}^{+\infty-iq} e^{\Psi(z)} \mathcal{F}[g](z, k) dz \quad \text{recall (7.14)} \\ &= -\frac{1}{2\pi} \int_{-\infty-iq}^{+\infty-iq} \frac{1}{z^2} e^{-izk + \Psi(z)} dz \\ &= \frac{1}{2\pi} \int_{-\infty+iq}^{+\infty+iq} \frac{-1}{z^2} e^{izk + \Psi(-z)} dz\end{aligned}$$

The same development holds for $E[(X - k)^-]$. □

The error function $ER(k, q)$ between the call payoff and the inverse Fourier (7.16) is defined as follows.

$$ER(k, q) = \sqrt{\frac{1}{m} \sum_{j=1}^m [(x_j - k)^+ - \check{g}(x_j, k)]^2} \quad \text{with } -M \leq x_j \leq M, \quad M > 0 \quad (7.17)$$

Where k (strike price) and q (parameter) are the inputs of the function $ER(k, q)$. The parameter q is used to optimize the function $ER(k, q)$. Fig 7a shows how the accuracy of the inverse Fourier (7.16) depends on the parameter q .

Fig 7b displays the $ER(k, q)$ minimum value (in blue color) as a function of the strike price (k); the correspondent optimal parameter (q) is graphed as a function of the strike price (k) in Fig 7b. The $ER(k, q)$ minimum value oscillates between $1.337 * 10^{-4}$ and $1.650 * 10^{-4}$, which is almost zero. The optimal parameter (q) decreases slowly from -0.0576 to -0.0567 as shown Fig 7b.

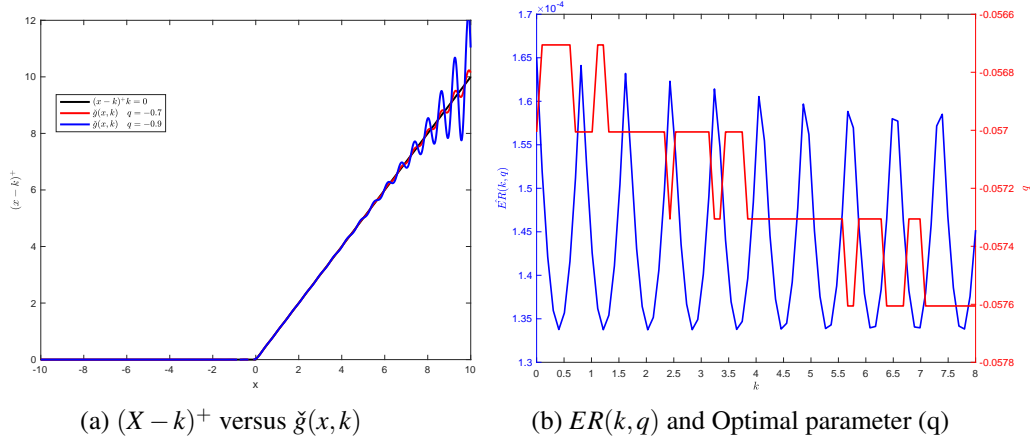


FIGURE 7. Optimal parameter (q) and minimum Error value ($ER(k, q)$)

Corollary 7.2

X is a GTS($\mu, \beta_+, \beta_-, \alpha_+, \alpha_-, \lambda_+, \lambda_-$) random variable with characteristic exponent function $\Psi(\xi)$.

There exists $q > 0$ such that

$$\begin{aligned}
 AVaR_{1-\alpha}(X) &= VaR_{1-\alpha}(X) + \frac{1}{1-\alpha} \frac{1}{2\pi} \int_{-\infty+iq}^{+\infty+iq} \frac{-1}{z^2} e^{izVaR_{1-\alpha}(X)+\Psi(-z)} dz & \alpha > \frac{1}{2} \\
 AVaR_{\alpha}(X) &= VaR_{\alpha}(X) + \frac{1}{\alpha} \frac{1}{2\pi} \int_{-\infty-iq}^{+\infty-iq} \frac{1}{z^2} e^{izVaR_{\alpha}(X)+\Psi(-z)} dz & \alpha < \frac{1}{2}
 \end{aligned} \tag{7.18}$$

Proof:

Equations (7.12) lead to equation (7.18) by substituting $k = VaR_{\alpha}(X)$ and applying theorem (7.1). \square

For tail probability (α) from 0.5%, 1%, ..., 10%, the theoretical and empirical Value-at-Risk ($VaR_{\alpha}(X)$) was computed and summarized in table 9 (appendix B.2). For the correspondent confidence Level ($1 - \alpha$) from 90%, ..., 99%, 99.5% the estimations of the the theoretical and empirical Value-at-Risk ($VaR_{1-\alpha}(X)$) are summarised in table 7. Both tables show that the empirical and theoretical Value-at-Risk are consistent. As expected, the bitcoin theoretical and empirical Value-at-Risk ($VaR_{1-\alpha}(X)$) are higher than that of the S&P 500 index, which is consistent with the heavy-tailedness of the bitcoin.

TABLE 7. Average Value-at-Risk Statistics

$AVaR_{1-\alpha}(X)$	S&P 500 (%)		Bitcoin (%)	
Confidence Level (α)	Empirical	Theoretical	Empirical	Theoretical
90%	1.8976	1.9278	7.3077	7.3190
91%	1.9730	2.0074	7.6273	7.6451
92%	2.0584	2.0971	7.9916	8.0130
93%	2.1585	2.1997	8.4150	8.4343
94%	2.2790	2.3193	8.9274	8.9259
95%	2.4304	2.4624	9.5154	9.5145
96%	2.6269	2.6399	10.2239	10.2448
97%	2.8887	2.8724	11.1451	11.2015
98%	3.3001	3.2070	12.3666	12.5767
99%	4.1403	3.7960	14.5488	14.9924
99.5%	5.2054	4.4047	16.9509	17.4790

To generalize the computation performed in table 7 & 9 and accounted for a large range of values, we consider the interval $[0, 10]$ for tail probability (α) in Fig 8b; and the interval $[90, 100]$ for confidence level ($1 - \alpha$) in Fig 8a. As illustrated in Fig 8a, the average value-at-risk ($AVaR_{1-\alpha}(X)$) of bitcoin and S&P 500 index increase at an increasing rate on both intervals, which justified concave nature of each curve.

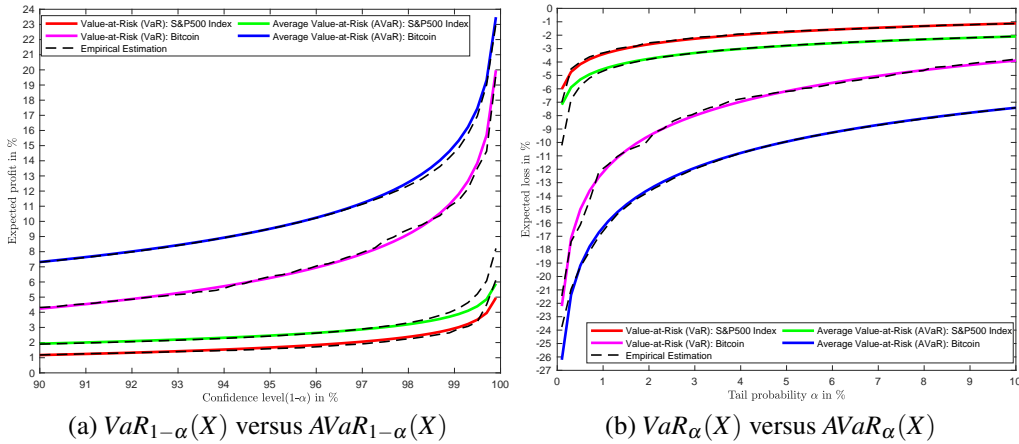


FIGURE 8. Average Value-at-Risk Statistics

The $AVaR_{1-0.999}(X) = 23.48\%$ for bitcoin and $AVaR_{1-0.999}(X) = 5.88\%$ for the S&P 500 index; and the tail probability(α), the $AVaR_{0.001}(X) = -26.21\%$ for bitcoin and $AVaR_{0.001}(X) = -7.18\%$ for the S&P 500 index. As shown in Fig 8, the left side of the tail probability generates higher value-at-risk ($VaR_{\alpha}(X)$) and average value-at-risk ($AVaR_{\alpha}(X)$) than the right side of tail probability for both bitcoin and S&P 500 index. At a risk level (α), the severity of the loss ($AVaR_{\alpha}(X)$) on the left side of the distribution is larger than the severity of the profit ($AVaR_{1-\alpha}(X)$) on the right side of the distribution. The result comes from the left-skewness nature of the distribution

for both bitcoin and S&P 500 index.

The magnitude of the discrepancy between the average value-at-risk ($AVaR_\alpha(X)$) of bitcoin and S&P 500 index can be evaluated by dividing the $AVaR_\alpha(X)$ of the Bitcoin by the $AVaR_\alpha(X)$ of the S&P 500 index and analyzed the relationship as shown in Fig 9.

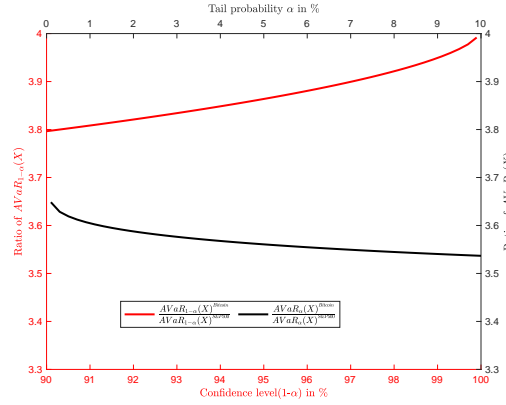


FIGURE 9. $\frac{AVaR_\alpha(X)^{Bitcoin}}{AVaR_\alpha(X)^{S\&P500}}$

The Profits generated by the average value-at-risk ($AVaR_{1-\alpha}(X)$) of bitcoin at one significant figure is four times larger than that of the S&P 500 index. Similarly, the losses generated by the average value-at-risk ($AVaR_\alpha(X)$) of bitcoin at one significant figure is four times larger than that of the S&P 500 index as shown in Fig 9.

8. CONCLUSION

The paper analyzes the daily return distribution of the bitcoin and S&P 500 index. It assesses their tail probabilities through the value-at-risk (VaR) and the average value-at-risk (AVaR). As a methodology, We use the historical prices for Bitcoin and S&P 500 index. The Bitcoin price spans from January 04, 2010, to June 16, 2023, and the S&P 500 index price period is from April 28, 2013, to June 22, 2023. Each historical data is used to fit the seven-parameter General Tempered Stable (GTS) distribution to the underlying data return distribution. The advanced Fast Fractional Fourier transform (FRFT) scheme is developed by combining the classic Fast Fractional Fourier (FRFT) algorithm with the 12-point rule Composite Newton-Cotes Quadrature. The advanced FRFT scheme is used to perform the Maximum likelihood estimation of the seven parameters of the GTS distribution and the computations derived from the GTS density and cumulation distribution functions. It results from the GTS distribution fitting that the stability indexes, the process intensities, and the decay rate are all positive, and the bitcoin return and S&P 500 index return are infinite activity processes with infinite jumps in any given time interval. The parameter analysis shows that the Bitcoin and S&P 500 index returns are left-skewed distributions. The study of the probability density function (pdf) and some Key Statistics show that the tail events of both Bitcoin and S&P 500 index are much more prevalent than we would expect with a Normal distribution. Both probability density functions are leptokurtic distributions. However, The heavy-tailedness is the main characteristic of the Bitcoin return, whereas the peakedness is the main characteristic

of the S&P 500 index return. The GTS distribution shows that 80.05% of S&P 500 returns are within -1.06% and 1.23% against only 40.32% of Bitcoin returns. The value-at-risk and the average value-at-risk reveal significant differences in tail probability between the Bitcoin returns and S&P 500 index returns. At a risk level (α), the severity of the loss ($AVaR_{\alpha}(X)$) on the left side of the distribution is larger than the severity of the profit ($AVaR_{1-\alpha}(X)$) on the right side of the distribution. Compared to the S&P 500 index, Bitcoin has 39.73% more prevalence to produce high daily returns (more than 1.23% or less than -1.06%). The severity analysis shows that at a risk level (α) the average value-at-risk ($AVaR(X)$) of the bitcoin returns at one significant figure is four times larger than that of the S&P 500 index returns at the same risk.

REFERENCES

- [1] Antony Lewis. *The basics of bitcoins and blockchains: an introduction to cryptocurrencies and the technology that powers them*. Mango Media Inc., 2018.
- [2] Satoshi Nakamoto. Bitcoin: A peer-to-peer electronic cash system. *Decentralized business review*, 2008.
- [3] Dirk G Baur and Thomas Dimpfl. The volatility of bitcoin and its role as a medium of exchange and a store of value. *Empirical Economics*, 61(5):2663–2683, 2021.
- [4] Dirk G Baur, KiHoon Jimmy Hong, and Adrian D Lee. Bitcoin—currency or asset? *Melbourne Business School*, 2016.
- [5] Ole Bjerg. How is bitcoin money? *Theory, culture & society*, 33(1):53–72, 2016.
- [6] David Yermack. Is bitcoin a real currency? an economic appraisal. In *Handbook of digital currency*, pages 31–43. Elsevier, 2015.
- [7] Lo Stephanie and Wang J Christina. Bitcoin as money. *Current Policy Perspectives*, (14-4), 2014.
- [8] Dirk G Baur, Kihoon Hong, and Adrian D Lee. Bitcoin: Medium of exchange or speculative assets? *Journal of International Financial Markets, Institutions and Money*, 54:177–189, 2018.
- [9] Pavel Ciaian, Miroslava Rajcaniova, and d’ Artis Kancs. The economics of bitcoin price formation. *Applied economics*, 48(19):1799–1815, 2016.
- [10] Dimitrios Koutmos. Investor sentiment and bitcoin prices. *Review of Quantitative Finance and Accounting*, 60(1):1–29, 2023.
- [11] Conghui Chen, Lanlan Liu, and Ningru Zhao. Fear sentiment, uncertainty, and bitcoin price dynamics: The case of covid-19. *Emerging Markets Finance and Trade*, 56(10):2298–2309, 2020.
- [12] Rodrigo Hakim das Neves. Bitcoin pricing: impact of attractiveness variables. *Financial Innovation*, 6(1):21, 2020.
- [13] Dilip B Madan, Peter P Carr, and Eric C Chang. The variance gamma process and option pricing. *Review of Finance*, 2(1):79–105, 1998.
- [14] A. H. Nzokem. Pricing european options under stochastic volatility models: Case of five-parameter variance-gamma process. *Journal of Risk and Financial Management*, 16(1), 2023.
- [15] A. H. Nzokem. Gamma variance model: Fractional fourier transform (FRFT). *Journal of Physics: Conference Series*, 2090(1):012094, nov 2021.
- [16] A.H. Nzokem and V.T. Montshiwa. The ornstein–uhlenbeck process and variance gamma process: Parameter estimation and simulations. *Thai Journal of Mathematics*, 21(3):160–168, Sep. 2023.
- [17] Uwe Küchler and Stefan Tappe. Tempered stable distributions and processes. *Stochastic Processes and their Applications*, 123(12):4256–4293, 2013.
- [18] A. H. Nzokem. European option pricing under generalized tempered stable process: Empirical analysis. arXiv.2304.06060[q-fin.PR], 2023.
- [19] Peter Carr, Hélyette Geman, Dilip B Madan, and Marc Yor. Stochastic volatility for lévy processes. *Mathematical finance*, 13(3):345–382, 2003.
- [20] Szymon Borak, Wolfgang Härdle, and Rafał Weron. Stable distributions. In *Statistical tools for finance and insurance*, pages 21–44. Springer, 2005.
- [21] Svetlana Boyarchenko and Sergei Z Levendorskii. *Non-Gaussian Merton-Black-Scholes Theory*, volume 9. World scientific, 2002.

- [22] Svetlozar T Rachev, Young Shin Kim, Michele L Bianchi, and Frank J Fabozzi. *Financial models with Lévy processes and volatility clustering*, volume 187. John Wiley & Sons, 2011.
- [23] Michele Leonardo Bianchi, Stoyan V Stoyanov, Gian Luca Tassinari, Frank J Fabozzi, and Sergio M Focardi. *Handbook of heavy-tailed distributions in asset management and risk management*. World Scientific, 2019.
- [24] A. H. Nzokem and V. T. Montshiwa. Fitting generalized tempered stable distribution: Fractional fourier transform (frft) approach. ARXIV.2205.00586[q-fin.ST], 2022.
- [25] David H Bailey and Paul N Swarztrauber. The fractional fourier transform and applications. *SIAM review*, 33(3):389–404, 1991.
- [26] A. H. Nzokem. Fitting infinitely divisible distribution: Case of gamma-variance model. arXiv.2104.07580[stat.ME], 2021.
- [27] A. H. Nzokem. *Stochastic and Renewal Methods Applied to Epidemic Models*. PhD thesis, York University , YorkSpace institutional repository, 2020.
- [28] A. H. Nzokem. Numerical solution of a gamma - integral equation using a higher order composite newton-cotes formulas. *Journal of Physics: Conference Series*, 2084(1):012019, nov 2021.
- [29] A. H. Nzokem. Sis epidemic model: Birth-and-death markov chain approach. *International Journal of Statistics and Probability*, 10(4):10–20, July 2021.
- [30] Paolo Giudici, Geof H Givens, and Bani K Mallick. *Wiley series in computational statistics*, volume 596. Wiley Online Library, 2013.
- [31] Paul S Horn. A measure for peakedness. *The American Statistician*, 37(1):55–56, 1983.
- [32] Błażej Kocharński. Does kurtosis measure the peakedness of a distribution? *Wiadomości Statystyczne. The Polish Statistician*, 67(11):43–61, 2022.
- [33] Peter H Westfall. Kurtosis as peakedness, 1905–2014. rip. *The American Statistician*, 68(3):191–195, 2014.
- [34] Young Shin Kim, Svetlozar Rachev, Michele Leonardo Bianchi, and Frank J Fabozzi. Computing var and avar in infinitely divisible distributions. 2009.
- [35] Svetlozar Todorov Rachev, Stoyan V Stoyanov, and Frank J Fabozzi. *Advanced stochastic models, risk assessment, and portfolio optimization: The ideal risk, uncertainty, and performance measures*. Wiley, 2008.
- [36] Hasan Fallahgoul. Quantile-based inference for tempered stable distributions monash cqfis working paper 2017–9. 2017.

APPENDIX A.1. GTS($\beta_+, \beta_-, \alpha_+, \alpha_-, \lambda_+, \lambda_-$) PARAMETER ESTIMATION BY NEWTON – RAPHSON ITERATION ALGORITHM (5.5)

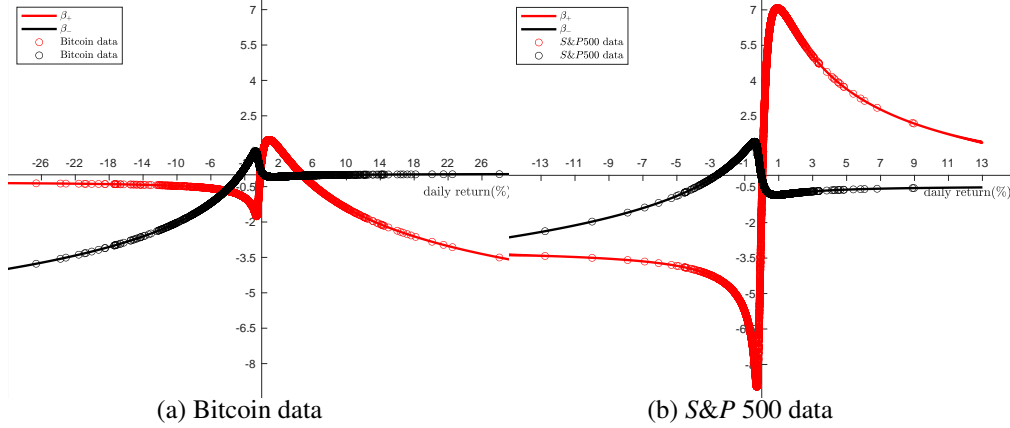


FIGURE 10. Stability indexes (β^+, β^-): $\frac{df(x,V)}{d\beta}$

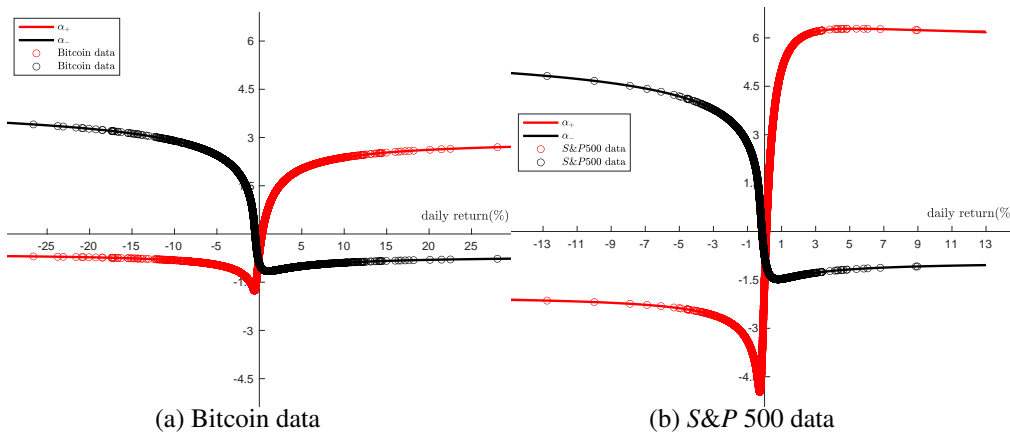


FIGURE 11. Process intensity (α^+, α^-): $\frac{df(x,V)}{d\alpha}$

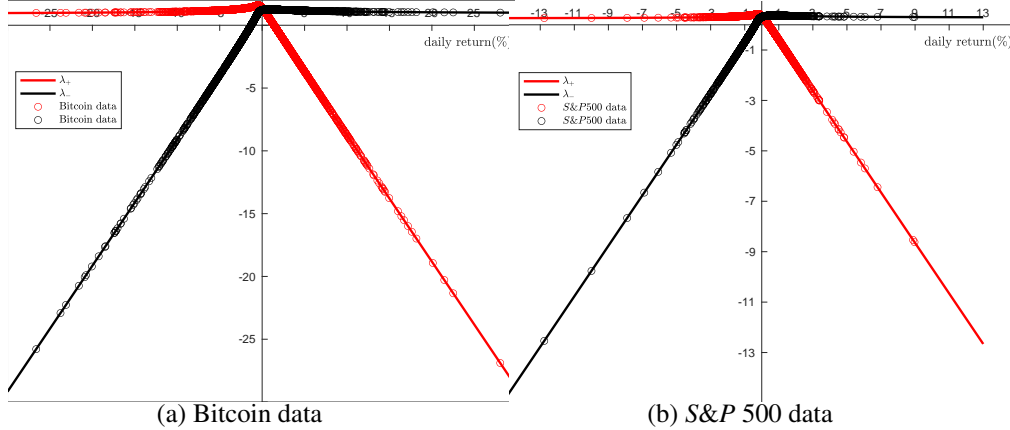


FIGURE 12. Tail decay rate (λ^+, λ^-): $\frac{df(x,V)}{d\lambda}$

APPENDIX B.2. VALUE-AT-RISK AND AVERAGE VALUE-AT-RISK

TABLE 8. Value-at-Risk Statistics

$VaR_\alpha(X)$	S&P 500 index (%)		Bitcoin (%)	
Confidence Level (α)	Empirical	Theoretical	Empirical	Theoretical
0.5%	-4.0015	-4.6199	-16.2620	-15.0205
1%	-3.2895	-3.4102	-11.9257	-12.2018
2%	-2.5580	-2.6769	-9.7612	-9.5086
3%	-2.1678	-2.2626	-7.7768	-7.9985
4%	-1.9143	-1.9766	-6.7164	-6.9609
5%	-1.7206	-1.7598	-6.1974	-6.1779
6%	-1.5858	-1.5863	-5.6524	-5.5536
7%	-1.4500	-1.4424	-5.1455	-5.0377
8%	-1.3183	-1.3201	-4.6358	-4.6002
9%	-1.2197	-1.2140	-4.1235	-4.2220
10%	-1.1301	-1.1207	-3.7848	-3.8903

TABLE 9. Average Value-at-Risk Statistics

$AVaR_{1-\alpha}(X)$	S&P 500 index (%)		Bitcoin (%)	
Confidence Level (α)	Empirical	Theoretical	Empirical	Theoretical
0.5%	-5.7738	-5.3096	-19.2754	-19.2164
1%	-4.6751	-4.5264	-16.6120	-16.3162
2%	-3.7955	-3.7627	-13.6827	-13.4993
3%	-3.3262	-3.3268	-11.9924	-11.8980
4%	-3.0149	-3.0233	-10.8089	-10.7862
5%	-2.7751	-2.7915	-9.9376	-9.9395
6%	-2.5867	-2.6047	-9.2719	-9.2587
7%	-2.4335	-2.4487	-8.7170	-8.6914
8%	-2.3029	-2.3152	-8.2367	-8.2067
9%	-2.1865	-2.1987	-7.8029	-7.7845
10%	-2.0846	-2.0955	-7.4088	-7.4114